

Structural and energetic properties of unsupported Cu nanoparticles from room temperature to the melting point: Molecular dynamics simulations

Francesco Delogu

Dipartimento di Ingegneria Chimica e Materiali, Università di Cagliari, piazza d'Armi, I-09123 Cagliari, Italy

(Received 20 June 2005; published 11 November 2005)

Molecular dynamics simulations have been employed to investigate the structure and the thermodynamics of unsupported Cu particles with size in the range between 1 and 10 nm. Carried out in the temperature range between 300 K and the melting point of the nanoparticle, the numerical study provides insight into the mechanisms governing the thermal evolution and melting of nanoparticles in the mesoscale regime explored. According to the numerical findings, nanoparticles can be regarded as heterogeneous structures characterized by a core region, in which atoms display a bulklike behavior, and a surface layer, where atoms possess structure and energy intermediate between the ones of a bulk solid or a bulk liquid.

DOI: [10.1103/PhysRevB.72.205418](https://doi.org/10.1103/PhysRevB.72.205418)

PACS number(s): 61.46.+w, 64.70.Nd, 82.60.Qr, 71.15.Pd

I. INTRODUCTION

Nanoscience is currently regarded as a fundamentally exciting and a technologically relevant area of research as a consequence of the novel physical and chemical behavior occurring on the nanoscale.^{1,2} For example, the thermodynamic properties of nanometer-sized systems are often largely different from the ones displayed by either coarse-grained matter or single atoms and molecules.¹⁻³ The system size affects these properties according to the so-called specific and smooth size effects.² The former is concerned with atomic clusters, which undergo an irregular variation of properties somehow related to “magic numbers.”^{2,4} The latter pertains instead to nanostructures in the size domain between small atomic clusters and infinite bulk systems,^{2,5} also referred to as the mesoscale regime. Within this broad size range, physical, and chemical properties typically change according to relatively simple scaling equations involving a power-law dependence on the system size.^{1-3,5} Such observations are generally explained with the high surface-to-volume ratio of nanoscale systems.¹⁻³ The consequent increased number of atoms at the surface of nanosized particles determines indeed a considerable surface energy contribution to the Gibbs free energy of the overall system.^{1,2,5}

The present work focuses on one of the most striking example of deviation of thermodynamic behavior as a consequence of a smooth size effect,^{1,2,5} i.e., the depression of the melting point of small particles of metallic species. The phenomenon was theoretically predicted by Pawlow in 1909 (Ref. 6) and further studied by Hollomon and Turnbull in 1953.⁷ Shortly after, it was subjected to experimental verification by Takagi,⁸ by means of transmission electron microscopy, and by Wronski and Coombes,^{9,10} who studied the relationship between the melting point of small metal particles and their size. It was found that the melting point decreases as the particle size decreases. This is generally regarded as a consequence of the size dependence of the chemical potential of atoms and molecules in finite systems.^{6,11-16} The phenomenon is satisfactorily accounted for by several phenomenological models,^{6,11-16} based on either the existence of a quasiliquid layer covering the surface

of the nanosized particle below the equilibrium melting point or the nucleation and growth of a liquid layer at the surface.^{6,11-16} These models are successful in that they predict the experimentally observed size dependence of the melting point.^{6,11-16} However, they are phenomenological and provide only a limited insight into the physical basis of the experimental behavior. As pointed out by Lai *et al.*,¹⁷ the comprehensive understanding of the thermodynamics of nanosized systems necessarily requires the experimental investigation of “the details of heat exchange during the melting process, in particular the latent heat of fusion.” Starting from this statement, Allen and co-workers developed an accurate experimental technique to properly investigate the calorimetry of the melting process in nanoparticles¹⁷⁻²⁰ and found in various systems that the melting point depression is accompanied by a reduction in the latent heat of transition.¹⁷⁻²⁰ It appears then that surface effects deeply affects the whole thermodynamic behavior, defining a complex framework of difficult understanding.

The present work attempts to further deepen the insight into the solid-to-liquid transition in nanometer-sized metal particles by employing molecular dynamics simulations. These have been successfully employed in the past to simulate the physical behavior of small metallic clusters, with size ranging in the interval between 13 and about 8000 atoms.²¹⁻²³ This work analyzes instead the behavior of particles in the so-called mesoscale regime, where no specific size effect should exist.^{1-3,23} Accordingly, the size of simulated systems ranges approximately from 5×10^2 to 6×10^4 atoms. Within this size range, the structural and energetic features of the nanoparticles were studied at increasing temperatures in order to characterize the properties of the surface layer and their influence on the melting process. Numerical simulation procedures are detailed in the following section.

II. COMPUTATIONAL METHODS

Calculations were carried out on systems of variable size consisting of Cu atoms. Interatomic potentials were described by a semi-empirical tight-binding force scheme based on the second-moment approximation to the electronic

density of states.^{24,25} It then follows that the cohesive energy E is equal to

$$E = \sum_{i=1}^N \left\{ \sum_{j=1}^N A e^{-p((r_{ij}/d)-1)} - \left[\sum_{j=1}^N \xi^2 e^{-2q((r_{ij}/d)-1)} \right]^{1/2} \right\}, \quad (1)$$

where r_{ij} is the distance between atoms i and j and the parameters A , ξ , p , and q quantify the interatomic potential between pairs of Cu atoms. The term d represents the nearest-neighbor distance and N the total number of atoms. The repulsive part of the potential is expressed in the first member on the right-hand side of Eq. (1) as a Born-Mayer pairwise interaction, while the attractive part is expressed in the second member within the framework of the second-moment approximation of tight-binding band energy.^{25,26} Interatomic potential parameter values were taken equal to the ones already reported in literature.²⁶ Interactions were computed for distances r_{ij} within a spherical cutoff radius $r_c=0.673$ nm, approximately corresponding to the seventh shell of neighbors.

The choice of the cutoff distance is connected with the necessity of reproducing with the highest possible accuracy the physical and chemical properties of the simulated system. At the same time, it is also necessary to avoid excessively cumbersome calculations, which rapidly grow with the number of interactions to compute for each atom. Actually, a cutoff distance at the fifth shell of neighbors is already sufficient to satisfactorily reproduce thermodynamic properties.²⁶ Elastic properties, more sensitive to long-range force fluctuations than thermodynamic quantities, are better estimated with longer cutoff distances.²⁶ Under suitable conditions, a cutoff radius $r_c=0.673$ nm permits the calculation of elastic constants with remarkable accuracy, reproducing experimental quantities within a 5% error.²⁶

It is here worth noting that the semiempirical tight-binding potential displays its best performances only for bulk interactions.^{24–26} Surface properties are indeed reproduced less satisfactorily than bulk ones. The Finnis-Sinclair potential²⁷ and the so-called embedded-atom-method²⁸ are, in this sense, more versatile. In spite of this, the tight-binding force scheme appears particularly suited for the simulations of face-centered-cubic (fcc) and hexagonal-close-packed (hcp) metallic structures.^{24–26} Even though it is not able to stabilize a body-centered-cubic (bcc) lattice, in the case of compact structures the tight-binding approach ensures an accurate reproduction of low-temperature as well as of high-temperature properties with the same set of potential parameters. In spite of its possible drawbacks in terms of accuracy for the evaluation of surface properties, the tight-binding potential appears then as one of the most natural choices for simulating fcc metals. In addition, it is also worth noting that the present study does not aim to a quantitative prediction of the physical and chemical behavior of Cu nanoparticles in the mesoscale regime, but rather to the qualitative exploration of the dynamics in connection with the occurrence of melting processes. Under such circumstances, the accurate reproduction of surface properties can be thus considered a secondary objective also in the light of the difficulties gen-

erally met with such objective in the field of numerical simulations.

Simulations were carried out within the so-called Nosè-Andersen (NPT) ensemble with the number of particles N , the temperature T and the pressure P constant.^{29,30} The so-called Parrinello-Rahman scheme was also implemented.³¹ The equations of motion were solved by applying a fifth-order predictor-corrector algorithm³² with a time step δt equal to 2.0×10^{-15} s.

Numerical calculations were initially performed on a system consisting of 562432 Cu atoms arranged in a cubic simulation box of $52 \times 52 \times 52$ face-centered-cubic (fcc) cells. Periodic boundary conditions were applied along the x , y , and z Cartesian directions to reproduce a perfect crystalline bulk. The system was relaxed at temperature $T=300$ K and external pressure $P \approx 0$ for 1×10^{-11} s, corresponding to 5×10^4 time steps.

Nanosized systems were prepared starting from the relaxed crystalline bulk consisting of 562 432 atoms arranged on the fcc $cF4$ structure. Approximately spherical portions of the crystalline bulk were individuated by considering one of the atoms in the central region of the bulk as the center of a sphere of radius R . The nanosized crystalline particle consisted of the atoms lying within the sphere of radius R , i.e., by the atoms within a distance R from the central one. The radius R was given the values corresponding to the odd multiples between 3 and 25 of the bulk lattice parameter a at 300 K, amounting to about 0.36 nm. Interactions between the atoms forming the nanoparticle and the ones outside were then gradually canceled to relax the nanocrystal, particularly at the surface. To do this, the values of the potential parameters A and ξ were reduced to zero according to a linear decreasing trend in 8×10^2 time steps for the pair interactions between the atoms of the nanoparticle and the external ones belonging to the parent fcc matrix. Independent simulations on the three smallest systems indicate that the nanocrystals obtained according to such procedure are characterized by a remarkably higher stability than the ones obtained by canceling the interactions between the nanoparticle and the parent matrix in a single time step. In the latter case, indeed, surface atoms in particular display considerable mobility and the whole particle undergoes marked fluctuations in density and shape, occasionally resulting in the occurrence of a solid-solid transition. These were easily pointed out by the so-called Honeycutt-Andersen parameters,³³ which identify the local crystalline order around each atom. On the three smallest systems analyzed, the sudden removal of the parent fcc matrix determines the formation of stacking faults. Domains with hcp order can be identified and a general increase of the icosahedral character of atomic arrangement is observed in agreement with previous studies.²³ Even though not completely absent, these phenomena are considerably reduced when interactions are gradually canceled. Shape fluctuations are significantly limited and smooth, although faceted, surfaces are obtained.

Simulations on nanocrystals were performed within the (NhT) ensemble with number of atoms N , shape h , and temperature T constant.^{23,32} The fcc nanocrystal was slowly heated to attain melting by imposing temperature jumps $\Delta T=10$ K and a relaxation after each temperature of 2

$\times 10^4$ time steps. The corresponding heating rate amounts to 250 K ns^{-1} . Following previously developed computational procedures,²³ the heat capacity $c_p(T)$ of the nanocrystal was evaluated according to the following equation:

$$c_p(T) = \frac{\partial U}{\partial T} + \frac{3}{2}R_{\text{gas}}, \quad (2)$$

where U is the average potential energy and R_{gas} the universal gas constant. The simulated $c_p(T)$ values were then locally best-fitted with suitable polynomial functions and the temperature at which the fitted curve attained its maximum value identified the melting point T_m of the nanocrystal.²³ The heat of fusion ΔH_m at the melting point T_m was evaluated as the difference at T_m between the potential energies of the liquid and the solid nanosized system.²³

The radius R_p of the nanocrystalline particle was estimated by employing the following expression:

$$R_p = R_g \left(\frac{5}{3} \right)^{1/2} + R_{\text{Cu}}, \quad (3)$$

where R_{Cu} represents the distance of nearest neighbors in Cu and

$$R_g = \left[\frac{1}{N} \sum_i (R_i - R_{\text{cm}})^2 \right]^{1/2} \quad (4)$$

is the radius of gyration, with R_{cm} representing the position of the center of mass of the nanocrystal.³²

The potential energy U was used to roughly distinguish between atoms with bulklike behavior and atoms affected by surface effects. Surface atoms are indeed expected to possess a potential energy higher than the atoms in the bulklike core of nanocrystals.¹⁻³ To properly identify bulklike atoms, potential energy was evaluated at the end of each relaxation stage between two consecutive temperature jumps starting from the center of the nanoparticle outward. More specifically, the procedure required initially the calculation of the average potential energies $U_b(r)$ for the atoms within a distance r from the center of the nanoparticle and $U_s(r)$ for the atoms in the external shell at distances in the range between r and R_p . The minimum r value considered was the one corresponding to the radial distance $r_{\text{min}}=0.305 \text{ nm}$ at which the radial distribution function of crystalline Cu has its first minimum at 300 K. The radius r was then changed from r_{min} to R_p with increments Δr . For sake of convenience, Δr was chosen equal to $r_{\text{min}}/2$. At each $r=r_{\text{min}}+n \Delta r$, with $n=0, 1, \dots$, the potential energies $U_b(r)$ and $U_s(r)$ were evaluated and compared. Of course, the total average potential energy U of the nanoparticle is given by the weighted sum of the two $U_b(r)$ and $U_s(r)$ contributions. The average potential energy of bulklike atoms $U_b(r)$ was also compared with the average potential energy U_{bulk} of atoms in a perfect crystalline bulk at the same temperature. A distance r_b can be thus roughly identified within which atoms display a bulklike behavior, with $U_b(r)$ approximately equal to U_{bulk} . At distances greater than r_b , the potential energy $U_b(r)$ undergoes instead marked deviations from U_{bulk} , assuming larger values. At the same time, the potential energy $U_s(r)$ of the external spheri-

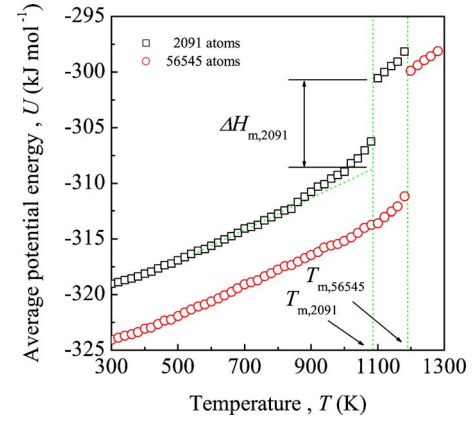


FIG. 1. (Color online) The average potential energy U as a function of temperature T for the nanoparticles consisting of 56 545 (lower curve) and 2091 (upper curve) atoms. Melting points T_m are indicated by vertical dotted lines. The linear extrapolations of data for the solid and liquid phases are also shown in the case of the system containing 2091 atoms in order to identify the latent heat of fusion ΔH_m .

cal shell shows a continuous variation as the radial distance r increases. The distance r_b can be therefore used to roughly separate atoms in the surface layer, characterized by relatively high potential energy $U_s(r)$, from those with bulklike behavior and average potential energy $U_b(r)$ approximately equal to the one of atoms in a perfect crystalline bulk. Correspondingly, the layer formed by surface atoms has a thickness $\Delta=R_p-r_b$.

The dynamics of bulklike and surface atoms was further analyzed by means of the average root-mean-square (rms) thermal displacement δ_r , defined as³²

$$\delta_r = \left[\frac{1}{N} \sum_{i=1}^N (\mathbf{r}_i - \mathbf{r}_{0,i})^2 \right]^{1/2}, \quad (5)$$

where \mathbf{r}_i is the vector defining the i th atom and $\mathbf{r}_{0,i}$ is the i th atom equilibrium position. The trajectories of single atoms were evaluated over a time period τ of 40 ps, with time intervals of 10 ps large enough for thermal diffusion to eventually occur. Average rms thermal displacements $\delta_{r,b}$ and $\delta_{r,s}$ were calculated, averaging over bulklike and surface atoms, respectively. The quantity $\delta_{r,b}$ is then referred to atoms within a distance r_b from the center of the nanocrystal, while $\delta_{r,s}$ is referred to atoms at distances between r_b and R_p , i.e., in the surface layer of thickness Δ .

III. RESULTS AND DISCUSSION

The gradual temperature increase determines a corresponding increase in the kinetic and potential energy of the nanocrystal. The typical trend of potential energy U as a function of temperature T is shown in Fig. 1 for the systems with 56 545 and 2091 Cu atoms. In the former case, the gradual increase of energy U is followed by a sudden upward jump, which clearly marks the occurrence of melting. A similar behavior also characterizes the latter case, concerning the system of 2091 atoms. However, the upward jump of poten-

TABLE I. Number of atoms N , particle radius R_p , melting point T_m , and latent heat of fusion ΔH_m for the systems investigated. The values obtained for nanoparticles must be compared with the experimental and numerically estimated ones also reported in the separate table below.

N	R_p , nm	T_m , K	ΔH_m , kJ mol ⁻¹
451	1.08	989	4.86
2091	1.80	1090	8.04
5746	2.52	1139	9.41
12213	3.24	1163	10.15
22303	3.96	1180	10.66
36810	4.68	1190	11.02
56545	5.40	1196	11.24
82316	6.12	1205	11.42
114921	6.84	1209	11.56
155165	7.56	1213	11.71
203854	8.28	1214	11.78
261790	9.10	1220	11.87
Bulk crystal	T_m , K	ΔH_m , kJ mol ⁻¹	
Experimental	1356	13.02	
Simulated	1250	12.57	

tial energy U is here preceded by a regular increase distributed over a relatively broad temperature range.

Although the melting point T_m is more accurately estimated by locating the maximum of the heat capacity $c_p(T)$ evaluated according to Eq. (2), data in Fig. 1 already point out that the system of smallest size possesses the lowest melting point T_m . This is also the case of the latent heat of fusion ΔH_m , corresponding to through the difference at T_m between the potential energy U of the liquid and solid nanoparticle. In analogy with the melting point T_m , the latent heat of fusion ΔH_m decreases as the system size decreases. The numerical estimates of both melting point T_m and latent heat of fusion ΔH_m are reported in Table I together with the corresponding size of the nanocrystals investigated. For sake of illustrations, the T_m and ΔH_m values are also reported in Figs. 2 and 3, respectively, as a function of the radius R_p of the nanoparticle.

A. Extension of bulklike core and surface regions

The radial profile of the average potential energy U suggests a rough distinction between bulklike and surface atoms. A typical example of the isothermal variation of the average potential energies $U_b(r)$ and $U_s(r)$ at 300 K along the radius r of the nanoparticle is shown in Fig. 4. Data pertain to the system of 22 303 atoms, which form a particle with a radius R_p of about 4 nm. While $U_s(r)$ undergoes a continuous change over the radial distance r , the potential energy $U_b(r)$ of the nanoparticle core region displays a nearly constant value roughly equal to U_{bulk} up to a radius r of about 3.1 nm. Beyond such value, the average potential energy $U_b(r)$ of core atoms begins to increase. For this reason, such radial distance is referred to as the boundary radius r_b approximately marking the boundary of atoms with bulklike behav-

ior and the surface layer. Surface atoms, therefore, are located in the external spherical shell about 0.8 nm thick.

Temperature has a relatively marked effect on various properties of the nanosized particles. For example, nanoparticles undergo a thermally induced volume expansion. As evident from Fig. 5, the radius R_p of the system with 22 303 atoms undergoes a small increase from 3.96 nm at 300 K to 4.13 nm at the melting point T_m of 1180 K. The thickness Δ of the surface layer, and then the radius r_b of the bulklike core, also depend on temperature. Of course, to properly determine boundary radius r_b , at each temperature T the average potential energy $U_b(r_b)$ of the core region has to be compared with the average potential energy U_{bulk} of the perfect crystalline bulk at the same temperature. As shown in Fig. 6

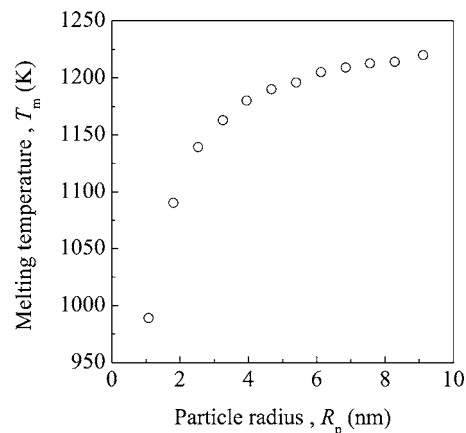


FIG. 2. The melting points T_m of the nanoparticles considered as a function of the particle radius R_p at 300 K. Data arrange according to a smooth trend, the lowest melting points pertaining to the smallest systems.

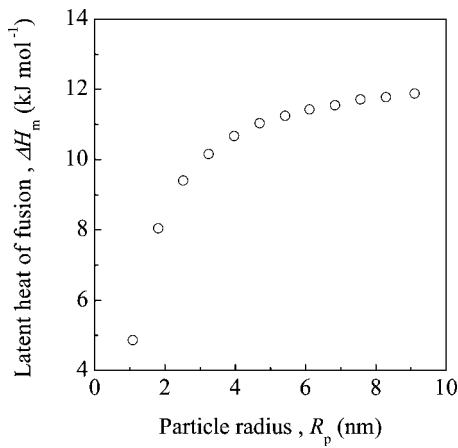


FIG. 3. The latent heats of fusion ΔH_m of the nanoparticles considered as a function of the particle radius R_p at 300 K. As in the case of the melting point T_m , ΔH_m values decrease as the system size decrease.

for the particle consisting of 261 790 atoms, the surface layer thickness Δ increases from about 0.37 to about 0.5 nm in the temperature range between 300 and 1220 K, the melting point for the nanosized system considered.

The thickness Δ of the surface layer is remarkably sensitive to the system size. This can be clearly seen from Fig. 7, where the Δ values at 300 K for the various systems investigated are reported as a function of the nanoparticle radius

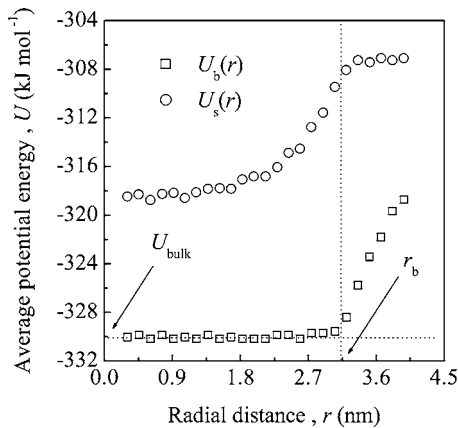


FIG. 4. The average potential energies $U_b(r)$ and $U_s(r)$ of the core region of radius r and of the external region of thickness $\Delta = R_p - r$, respectively, as a function of the radial distance r . The average potential energy U_{bulk} of the bulk solid at 300 K is indicated by the horizontal dotted line. It appears that the average potential energy $U_b(r)$ of the core region roughly coincides with the one of the bulk solid U_{bulk} up to a radius r_b of about 3.1 nm, indicated by the vertical dotted line. Marked deviations of $U_b(r)$ from U_{bulk} are instead observed at radial distances r larger than r_b . The average potential energy $U_s(r)$ of the external shell undergoes a smooth increase up to the radius r_b , keeping an approximately constant value at larger r . These features permit us to distinguish between a bulklike core region and a surface layer with different properties. The radial distance r_b can be then regarded as the boundary between bulklike and surface behavior. Data refer to the system of 22 303 atoms.

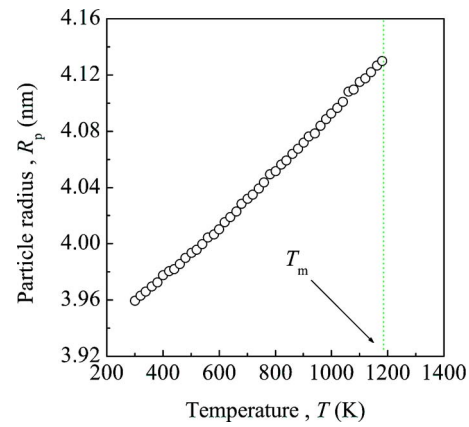


FIG. 5. (Color online) The change of the particle radius R_p as a function of temperature T from 300 K to the melting point T_m . The latter is indicated by the vertical dotted line. The particle radius undergoes a smooth, approximately linear increase as the temperature increases. Data refer to the system of 22 303 atoms.

R_p . The thickness Δ of the surface layer changes smoothly from about 0.9 to about 0.4 nm. Although limited in size to the R_p range approximately between 1 and 10 nm, data in Fig. 7 clearly point out that the surface layer thickness Δ grows inversely with the size of the nanoparticle. The surface layer thickness Δ pertain indeed to the smallest particles.

It is here worth noting that the data in Fig. 7 refer to systems of different size R_p but at the same temperature of 300 K, a temperature markedly lower than their melting point T_m . This evidence suggests that the observed variation of the surface layer thickness Δ should be ascribed to curvature effects. Thermal effects are indeed equal for all the investigated systems. Unfortunately, it has not been possible to explore the dynamics of systems with a number of atoms larger than about 262 000 due to limitations in the computational power available. It is therefore not clear if the surface layer thickness Δ regularly decreases up to very low values at large particle radii or attains instead an approximately constant value below a certain particle radius. This aspect certainly deserves further investigation.

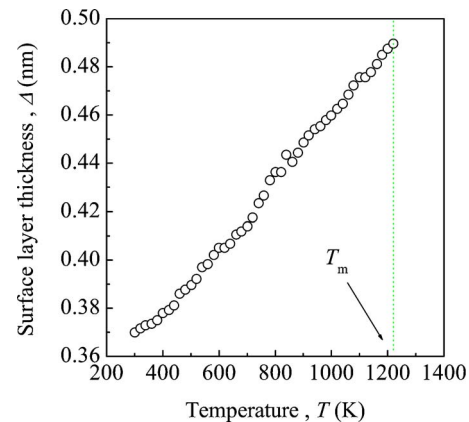


FIG. 6. (Color online) The dependence of the surface layer thickness Δ on the temperature T in the range between 300 K and the melting point T_m , indicated by the vertical dotted line. The surface layer thickness increases regularly as the temperature increases. Data refer to the system of 261 790 atoms.

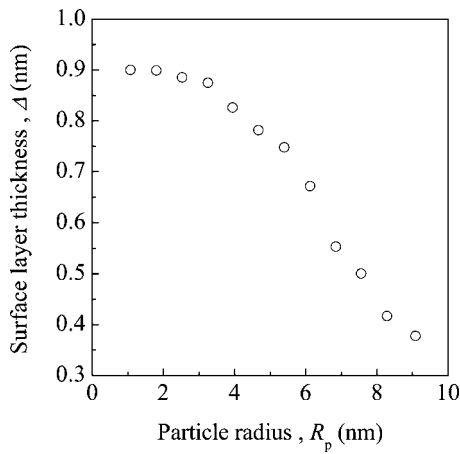


FIG. 7. The dependence of the surface layer thickness Δ on the particle radius R_p at 300 K. A monotonic decrease of the surface layer thickness is observed as the system size increases.

The thickness Δ of the surface layer attained at the melting point T_m is reported for each system as a function of the system size in Fig. 8. The same Δ data are quoted in Fig. 9 as a function of the melting point T_m of each nanocrystalline particle. Of course, the two figures show a set of data of surface layer thickness Δ affected by both curvature and thermal effects. The largest values of surface layer thickness Δ still pertain to the smallest particles. However, the fact that smallest particles melt at the lowest temperatures and, conversely, largest systems display the highest melting points determines a reduction in the difference between the surface layer thickness Δ of small and large particles. The latter systems are indeed characterized by a surface layer slightly thicker than the one attained at 300 K as a consequence of their relatively high melting points. Therefore, thermal effects slightly reduce the difference between the smallest and the largest values of surface layer thickness Δ due to the difference in melting point between the systems investigated.

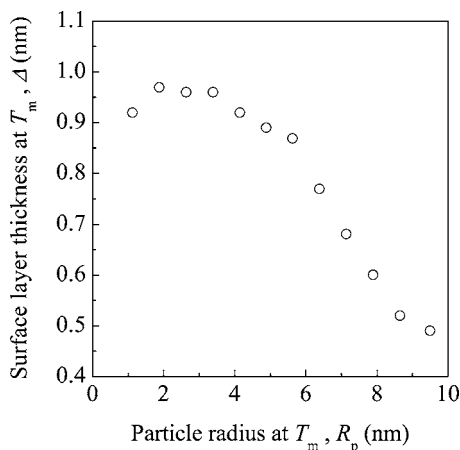


FIG. 8. The thickness Δ of the surface layer at the melting point T_m as a function of the particle radius R_p at the same temperature. A monotonic decrease is observed as in the case of data referred to 300 K.

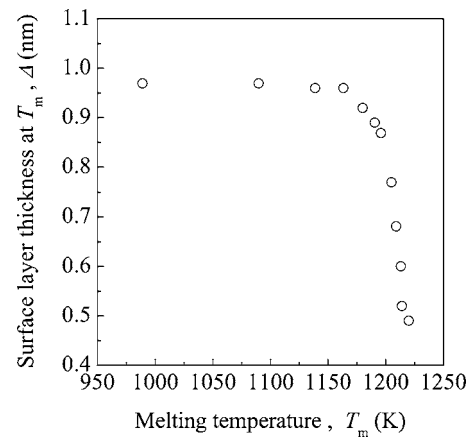


FIG. 9. The thickness Δ of the surface layer at the melting point T_m as a function of the melting point T_m . The thickness Δ of the surface layer undergoes a monotonic decrease.

B. Energy of bulklike core and surface regions

The estimation of the thickness Δ of the surface layer permits to roughly distinguish between bulklike and surface atoms and then to evaluate the average potential energy $U_s(r_b)$ possessed by surface atoms. The $U_s(r_b)$ values for the surface atoms of a nanoparticle of 261 790 atoms and a radius R_p of about 10 nm are shown in Fig. 10 as a function of temperature T . Quite surprisingly, the average potential energy $U_s(r_b)$ is only weakly dependent on temperature. On the contrary, the average potential energy of bulklike atoms $U_b(r_b)$, also reported in Fig. 10 for sake of comparison, displays as usual a definite dependence, increasing steadily with temperature. The increase of the average potential energy

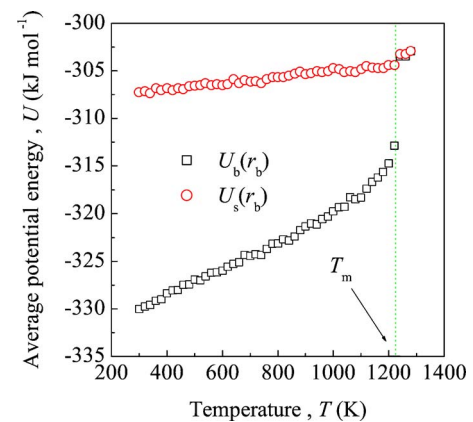


FIG. 10. (Color online) The average potential energies $U_b(r_b)$ and $U_s(r_b)$ of the bulklike core region of radius r_b and of the surface layer of thickness Δ as a function of the temperature T . It can be seen that the two quantities change at different rates, the highest one pertaining to $U_b(r_b)$. While $U_s(r_b)$ displays an approximate linearity over the whole temperature range explored, at temperatures close to T_m $U_b(r_b)$ shows a nonlinear behavior. At melting, $U_b(r_b)$ undergoes a sudden upward jump the amplitude of which is larger than the one undergone by the potential energy of surface atoms. The average potential energy $U_s(r_b)$ is indeed remarkably close to the one of the liquid. Data refer to the system of 261 790 atoms.

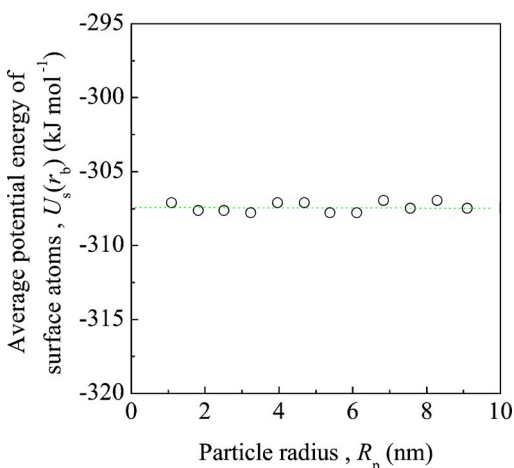


FIG. 11. (Color online) The average potential energy $U_s(r_b)$ of surface atoms at 300 K as a function of the particle radius R_p for the systems investigated. The almost constant value observed points out that the quantity $U_s(r_b)$ is independent of the system size.

$U_s(r_b)$ of surface atoms appears extremely small when compared to the one showed by $U_b(r_b)$.

It is worth noting that the average potential energy $U_s(r_b)$ of surface atoms corresponds to the one possessed by either a perfect crystalline bulk at a temperature of about 1490 K or a bulk liquid at about 1100 K. In the former case, the crystalline bulk would show a superheating of about 240 K with regard to the Cu equilibrium melting point, which amounts approximately to 1250 K for the tight-binding interatomic potential used in this study.³⁴ In the latter case, instead, the bulk liquid would show an undercooling of about 150 K. Under such circumstances, the energy state of the atoms in the surface layer is intermediate between the ones pertaining to an undercooled liquid and a superheated solid. At least at temperatures far from the melting point, their arrangement should be then regarded as amorphouslike rather than as liquidlike.

Further support to such interpretation is given by the relationship between the average potential energy $U_s(r_b)$ of surface atoms and the size of nanoparticles at a given temperature. The average potential energy $U_s(r_b)$ of surface atoms is indeed approximately insensitive to the radius R_p of the systems investigated, as shown by the plot of $U_s(r_b)$ as a function of R_p reported in Fig. 11.

The data quoted in Fig. 11 refer to systems at 300 K, but the same behavior is observed at higher temperatures. However, when the temperature increases the average potential energy $U_s(r_b)$ of the surface layer closely approaches the average potential energy of the liquid nanoparticle at its characteristic, size-dependent melting point T_m . This means that no net discontinuity in the potential energy of surface atoms is observed at melting. This suggests in turn that the atomic arrangement at the surface could undergo a structural softening interpretable as a premelting of the external shell, thus supporting the hypothesis that melting nucleates at external surfaces and then propagates in the interior of the particles.¹⁻³

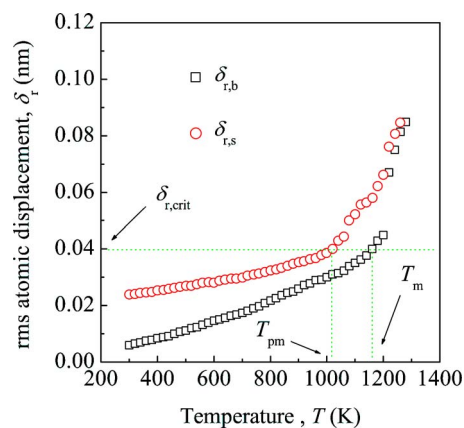


FIG. 12. (Color online) The rms atomic displacements $\delta_{r,b}$ and $\delta_{r,s}$ of bulklike and surface atoms, respectively, as a function of temperature T . The quantity $\delta_{r,s}$ is always larger than $\delta_{r,b}$, indicating that the structure of the surface layer is more disordered than the one of the bulklike core region. As usual, the rms atomic displacement increases as temperature increases. $\delta_{r,b}$ increases at rates higher than $\delta_{r,s}$. The horizontal line in the figure indicates the Lindemann threshold $\delta_{r,crit}$. The vertical lines indicate, instead, the temperatures T_{pm} and T_m at which surface and bulklike atoms attain such value. Data refer to the system of 12 213 atoms.

C. Structural arrangement of atoms in bulklike core and surface regions

The rms displacement δ_r of atomic species from their equilibrium positions provides a measure of the structural arrangement of atoms in the bulklike core region as well as in the surface layer.^{23,32} The two regions into which a particle can be roughly divided, so recognizing the existence of atoms with and without bulklike behavior, are indeed characterized by different values of the rms atomic displacement. As expected on the basis of the findings discussed above, bulklike atoms possess rms displacements $\delta_{r,b}$ smaller than the ones $\delta_{r,s}$ displayed by atoms in the surface layer of thickness Δ . As evident from the data reported in Fig. 12, relative to the case of a nanoparticle of radius R_p of about 3.5 nm and 12 213 atoms, the rms displacement $\delta_{r,s}$ of surface atoms is larger than the rms displacements $\delta_{r,b}$ of bulklike atoms at any temperature T . The difference between the two values decreases as temperature increases, indicating that the structure of the bulklike core is more sensitive to thermal disordering than the one of the surface layer, which is already considerably disordered. However, at temperatures relatively close to the melting point T_m , $\delta_{r,s}$ assumes values markedly higher than the ones displayed at lower temperatures and characteristic of a bulk liquid at the same temperatures. Such evidence strongly suggests the occurrence of premelting phenomena at the surface of the nanoparticle and the consequent formation of a liquidlike layer in which atomic species have a mobility analogous to the one displayed in a thermodynamically stable liquid phase. The data in Fig. 12 also show that the atomic species in the two bulklike and surface regions reach approximately the same value of rms atomic displacement only a few degrees above the melting point T_m , i.e., when also the bulklike region has melted.

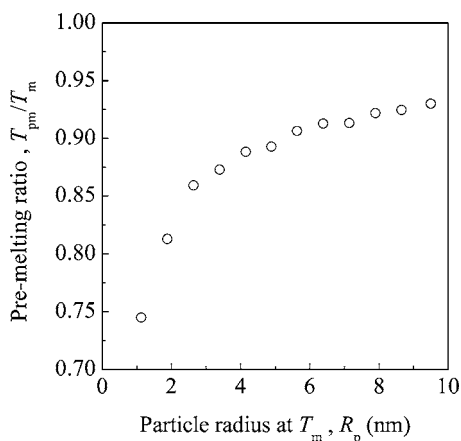


FIG. 13. The ratio between premelting temperature T_{PM} and melting point T_m as a function of the particle radius R_p at T_m for the systems investigated. The premelting ratio decreases regularly as the system size decreases. Premelting phenomena are then more pronounced in small particles than in large ones.

Lindemann-like criteria can be chosen to distinguish between melted and nonmelted regions on the basis of the rms displacement.²³ While the choice of the critical value of rms displacement beyond which a region has melted obviously affects the quantitative evaluation of the temperature at which premelting phenomena occur at the surface, it does not change the qualitative features of the phenomenon. Following previous studies,³⁵ a critical $\delta_{r,crit}$ threshold value of 0.04 nm has been here considered, which corresponds to about the 15% of the nearest-neighbors distance in Cu. According to such choice, the melting point T_m of the particle of 12 213 atoms amounts to about 1140 K, in satisfactory agreement with the T_m value of 1163 K obtained from the $c_p(T)$ curve. The surface layer instead undergoes melting at a temperature T_{PM} of about 1015 K, i.e., approximately 150 K below the melting point T_m of the bulklike region.

The premelting temperature T_{PM} at which surface atoms display a liquidlike behavior is affected by the system size. The plot of the ratio between premelting temperatures T_{PM} and melting points T_m , also referred to as the premelting ratio, as a function of the particle radius R_p is shown in Fig. 13. The premelting ratio decreases as the systems size decreases, thus indicating that pre-melting effects are more pronounced in the smallest particles.

The rms displacement $\delta_{r,s}$ of surface atoms is only slightly dependent on the size of the nanoparticle. This can be clearly seen in Fig. 14, where the $\delta_{r,s}$ values at 300 K are reported as a function of the particle radius R_p for all the systems investigated. The rms atomic displacement increases from 0.022 to 0.029 nm as the particle size changes from about 1 to about 10 nm. Surface curvature effects are then less pronounced than in the case of the surface layer thickness Δ .

IV. CONCLUSIONS

The use of molecular dynamics simulations permitted the extensive study of structural and energetic features of Cu

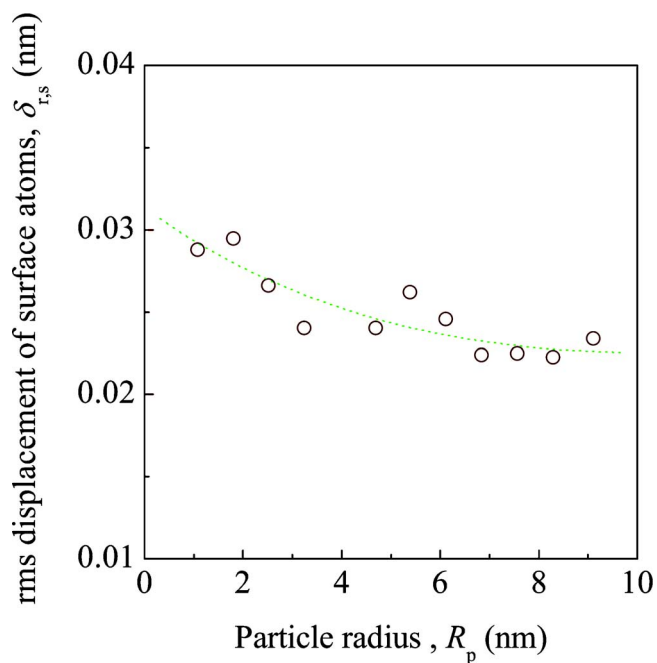


FIG. 14. (Color online) The rms atomic displacement $\delta_{r,s}$ of surface atoms as a function of the particle radius R_p at 300 K. An approximately constant value of about 0.024 nm is observed irrespective of the system size.

nanocrystals of different size in the so-called mesoscale regime between 1 and 10 nm. Structural and energetic properties were characterized in the temperature range between the room temperature and the melting point of each nanosized particle. In agreement with previous experimental findings and theoretical expectations, the melting point as well as the latent heat of fusion have been found dependent on the system size. In particular, both the thermodynamic quantities decrease as the particle size decreases.

Numerical simulations indicate that each nanocrystal can be roughly divided into two regions. In the core region, atoms display a behavior analogous to the one characteristic of atomic species in a perfect crystalline bulk. Atoms belonging to the surface layer possess instead potential energy and structural features suggesting an amorphouslike arrangement, i.e., an arrangement intermediate between the ones of a bulk solid and of a bulk liquid.

Both thermal and size effects affect surface atoms. The thickness of the surface layer is particularly sensitive to the system size, increasing as the particle size decreases. Conversely, the potential energy of surface atoms undergoes only a slight increase. Contrary to what happens to the potential energy of bulklike atoms, no discontinuity is observed at the melting point or in the neighborhood. This suggests that while the solid-to-liquid transition in the bulklike core is of the first order, the surface layer undergoes a melting transition with second-order features.

This conclusion is further supported by the evidence that surface atoms are subjected to premelting phenomena at temperatures well below the estimated melting point of the nanosized systems. The analysis of rms atomic displacements in the bulklike core and surface regions points out, indeed, that

surface atoms are characterized by higher mobility than bulklike ones. The mobility increases gradually, thus indicating that the surface layer undergoes a sort of structural softening.

The results obtained in the present work demonstrate that a nanosized particle can be regarded as a structurally and energetically heterogeneous system consisting of well distinct bulklike and surface regions. Further progress in the understanding of the atomic behavior on the nanoscale is

however expected from the simulation of larger systems, with sizes in the range of decades of nanometers.

ACKNOWLEDGMENTS

Dr. G. Manai is gratefully acknowledged for useful discussions. Professor P. Demontis and Professor G. B. Suffritti are gratefully acknowledged for the computational resources made available. The research was supported by the University of Cagliari.

-
- ¹P. Moriarty, Rep. Prog. Phys. **64**, 297 (2001).
 - ²J. Jortner and C. N. R. Rao, Pure Appl. Chem. **74**, 1491 (2002).
 - ³T. L. Hill, Nano Lett. **1**, 273 (2001).
 - ⁴M. Schmidt, R. Kusche, B. von Issendorf, and H. Haberland, Nature (London) **393**, 238 (1998).
 - ⁵P. Alivisatos, Science **271**, 933 (1996).
 - ⁶P. Pawlow, Z. Phys. Chem. (Munich) **65**, 1 (1909).
 - ⁷T. H. Hollomon and D. Turnbull, Prog. Met. Phys. **4**, 333 (1953).
 - ⁸M. Takagi, J. Phys. Soc. Jpn. **9**, 359 (1954).
 - ⁹C. R. M. Wronski, Br. J. Appl. Phys. **18**, 1731 (1967).
 - ¹⁰C. J. Coombes, J. Phys. F: Met. Phys. **2**, 441 (1972).
 - ¹¹K.-J. Hanszen, Z. Phys. **157**, 523 (1960).
 - ¹²Ph. Buffat and J.-P. Borel, Phys. Rev. A **13**, 2287 (1976).
 - ¹³P. R. Couchman and W. A. Jesser, Nature (London) **269**, 481 (1977).
 - ¹⁴H. Reiss, P. Mirabel, and R. L. Whetten, J. Phys. Chem. **92**, 7241 (1988).
 - ¹⁵H. Sakai, Surf. Sci. **351**, 285 (1996).
 - ¹⁶K. F. Peters, J. B. Cohen, Y.-W. Chung, Phys. Rev. B **57**, 13430 (1998).
 - ¹⁷S. L. Lai, J. Y. Guo, V. Petrova, G. Ramanath, L. H. Allen, Phys. Rev. Lett. **77**, 99 (1996).
 - ¹⁸M. Yu. Efremov, F. Schiettekatte, M. Zhang, E. A. Olson, A. T. Kwan, R. S. Berry, and L. H. Allen, Phys. Rev. Lett. **85**, 3560 (2000).
 - ¹⁹M. Zhang, M. Yu. Efremov, F. Schiettekatte, E. A. Olson, A. T. Kwan, S. L. Lai, T. Wisleder, J. E. Greene, L. H. Allen, Phys. Rev. B **62**, 10548 (2000).
 - ²⁰E. A. Olson, M. Yu. Efremov, M. Zhang, Z. Zhang, and L. H. Allen, J. Appl. Phys. **97**, 034304 (2005).
 - ²¹B. D. Hall, M. Flueli, R. Monot, and J.-P. Borel, Phys. Rev. B **43**, 3906 (1991).
 - ²²C. L. Cleveland, W. D. Luedtke, and U. Landman, Phys. Rev. B **60**, 5065 (1999).
 - ²³Y. Qi, T. Çağın, W. L. Johnson, and W. A. Goddard III, J. Chem. Phys. **115**, 385 (2001).
 - ²⁴F. Ducastelle, J. Phys. (Paris) **31**, 1055 (1970).
 - ²⁵V. Rosato, M. Guillope, and B. Legrand, Philos. Mag. A **59**, 321 (1989).
 - ²⁶F. Cleri, V. Rosato, Phys. Rev. B **48**, 22 (1993).
 - ²⁷M. W. Finnis, and J. F. Sinclair, Philos. Mag. A **50**, 45 (1984).
 - ²⁸M. S. Daw, M. I. Baskes, Phys. Rev. B **29**, 6443 (1984).
 - ²⁹H. C. Andersen, J. Chem. Phys. **72**, 2384 (1980).
 - ³⁰S. Nosè, J. Chem. Phys. **81**, 511 (1984).
 - ³¹M. Parrinello and A. Rahman, J. Appl. Phys. **52**, 7182 (1981).
 - ³²M. P. Allen and D. Tildesley, *Computer Simulation of Liquids* (Clarendon Press, Oxford, 1987).
 - ³³J. D. Honeycutt, H. C. Andersen, J. Phys. Chem. **91**, 4950 (1987).
 - ³⁴F. Delogu, Mater. Sci. Eng., A **403**, 48 (2005).
 - ³⁵J. J. Gilvarry, Phys. Rev. **102**, 308 (1956).